

# Higgs boson production in photon-photon interactions with proton, light-ion, and heavy-ion beams at current and future colliders

David d'Enterria<sup>a</sup>

CERN, EP Department, 1211 Geneva, Switzerland

Daniel E. Martins<sup>b</sup>

UFRJ, Univ. Federal do Rio de Janeiro, 21941-901, Rio de Janeiro, RJ

Patricia Rebello Teles<sup>c</sup>

ERJ, Univ. do Estado do Rio de Janeiro, 20550-900, Rio de Janeiro, RJ

(Dated: February 18, 2022)

The production of the Higgs boson in photon-photon interactions with proton and nucleus beams at three planned or proposed future CERN colliders — the high-luminosity Large Hadron Collider (HL-LHC), the high-energy LHC (HE-LHC), and the Future Circular Collider (FCC) — is studied. The cross sections for the process  $AA^{\gamma\gamma}(A)H(A)$ , with the ions  $A$  surviving the interaction and the Higgs scalar exclusively produced, are computed with MADGRAPH 5 modified to include the corresponding elastic  $\gamma$  fluxes, for Pb-Pb, Xe-Xe, Kr-Kr, Ar-Ar, O-O, p-Pb, and p-p over the nucleon-nucleon collision energy range  $\sqrt{s_{NN}} \approx 3\text{--}100$  TeV. Simulations of the  $\gamma\gamma \rightarrow H \rightarrow b\bar{b}$  decay mode — including realistic (mis)tagging and reconstruction efficiencies for the final-state b-jets, as well as appropriate kinematical selection criteria to reduce the similarly computed  $\gamma\gamma \rightarrow b\bar{b}, c\bar{c}, q\bar{q}$  continuum backgrounds — have been carried out. Taking into account the expected luminosities for all systems, the yields and significances for observing the Higgs boson in ultraperipheral collisions (UPCs) are estimated. At the HL-LHC and HE-LHC, the colliding systems with larger Higgs significance are Ar-Ar(6.3 TeV) and Kr-Kr(12.5 TeV) respectively, but  $3\sigma$  evidence for two-photon Higgs production would require 200 and 30 times larger integrated luminosities than those planned today at both machines. Factors of ten can be gained by running for a year, rather than the typical 1-month heavy-ion LHC operation, but the process will likely remain unobserved until a higher energy hadron collider, such as the FCC, is built. In the latter machine, the  $5\sigma$  observation of Higgs production in UPCs is feasible in just the first nominal run of Pb-Pb and p-Pb collisions at  $\sqrt{s_{NN}} = 39$  and 63 TeV respectively.

## I. INTRODUCTION

Heavy ions accelerated at high energies are surrounded by huge electromagnetic (e.m.) fields generated by the collective action of their  $Z$  individual proton charges. In the equivalent photon approximation (EPA) [1], such strong e.m. fields can be identified as quasireal photon beams with very low virtualities  $Q^2 < 1/R_A^2$  and large longitudinal energies of up to  $\omega_{\max} \approx \gamma_L/R_A$ , where  $R_A$  is the radius of the charge and  $\gamma_L = E_{\text{beam}}/m_{N,p}$  is the beam Lorentz factor for nucleon or proton mass  $m_{N,p} = 0.9315, 0.9382$  GeV [2, 3]. On the one hand, since the photon flux scales as the squared charge of each colliding particle, photon-photon cross sections are enhanced millions of times for heavy ions (up to  $Z^4 \approx 5 \cdot 10^7$  for Pb-Pb) compared to proton or electron beams. On the other, proton (and lighter ions) feature larger  $\omega_{\max}$  values thanks to their lower radii  $R_A$  and larger beam  $\gamma_L$  factors, and can thereby reach higher photon-photon center-of-mass (c.m.) energies. At the energies of the Large Hadron Collider (LHC), photons emitted from nuclei (with radii  $R_A \approx 1.2A^{1/3}$  fm) are almost on-shell (virtuality  $Q < 0.06$  GeV, for mass numbers  $A > 16$ ), and reach longitudinal energies of up to hundreds of GeV, whereas photon fluxes from protons ( $R_A \approx 0.7$  fm) have larger virtualities,  $Q \approx 0.28$  GeV, and longitudinal energies in the TeV range [3]. Table I summarizes the relevant characteristics of photon-photon collisions in ultraperipheral collisions (UPCs) of proton and nuclear beams at three planned or proposed CERN future hadron colliders: the high-luminosity LHC (HL-LHC) [4], the high-energy LHC (HE-LHC) [4, 5], and the Future Circular Collider (FCC) [6]. The beam luminosities for light- and heavy-ions considered here are those discussed in Refs. [4, 6]. Although the beam luminosities for p-p are 7 orders of magnitude larger than those for Pb-Pb, the running conditions with multiple pileup p-p collisions per bunch crossing hinder the measurement of exclusive  $\gamma\gamma$  events with central masses at 125-GeV (unless one installs, in the LHC case, very forward proton taggers at 420 m inside the tunnel, with 10-picosecond time resolution [7]). Thus,

<sup>a</sup> email: david.d'enterria@cern.ch

<sup>b</sup> email: dan.ernani@gmail.com

<sup>c</sup> email: patricia.rebello.teles@cern.ch

for p-p collisions in the present study we take  $\mathcal{L}_{\text{int}} = 1 \text{ fb}^{-1}$  as the value potentially integrated under low-pileup conditions that allow the reconstruction of exclusive photon-photon final states. In all cases in Table I, one can see that the maximum photon-photon c.m. energy reaches above the kinematical threshold for Higgs boson production,  $\sqrt{s_{\gamma\gamma}^{\text{max}}} \gtrsim m_H = 125 \text{ GeV}$ , through the process depicted in Fig. 1 (left). The observation of the  $\gamma\gamma \rightarrow H$  process would provide an independent measurement of the H-photon loop-induced coupling based not on the Higgs decay (as measured at the LHC [8]) but on its  $s$ -channel production mode.

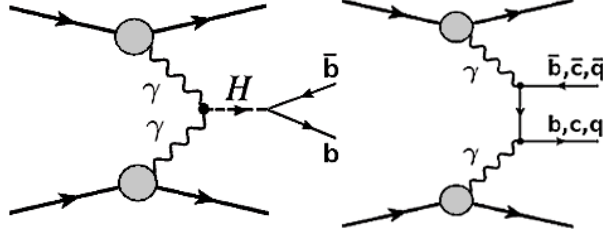


FIG. 1. Diagrams for the exclusive two-photon production of the Higgs boson (followed by its  $b\bar{b}$  decay, left), and of  $b$ -,  $c$ -, light-quark pairs (processes that share the same final state as the Higgs case, right) in ultraperipheral proton/nuclear collisions.

TABLE I. Summary of the characteristics of photon-photon collisions in ultraperipheral proton and nuclear collisions at the HL-LHC, HE-LHC, and FCC [4–6]: (i) Nucleon-nucleon c.m. energy  $\sqrt{s_{\text{NN}}}$ , (ii) integrated luminosity per run  $\mathcal{L}_{\text{int}}$ , (iii) beam energies  $E_{\text{beam}}$ , (iv) Lorentz factor  $\gamma_L$ , (v) effective charge radius  $R_A$ , (vi) photon “maximum” energy  $\omega_{\text{max}}$  in the c.m. frame, and (vii) “maximum” photon-photon c.m. energy  $\sqrt{s_{\gamma\gamma}^{\text{max}}}$ . The last two columns list the  $\gamma\gamma \rightarrow H$  cross sections and the expected number of Higgs events for the quoted  $\mathcal{L}_{\text{int}}$  per system.

System	$\sqrt{s_{\text{NN}}}$	$\mathcal{L}_{\text{int}}$	$E_{\text{beam1}} + E_{\text{beam2}}$	$\gamma_L$	$R_A$	$\omega_{\text{max}}$	$\sqrt{s_{\gamma\gamma}^{\text{max}}}$	$\sigma(\gamma\gamma \rightarrow H)$	$N(\gamma\gamma \rightarrow H)$
Pb-Pb	5.5 TeV	10 nb $^{-1}$	2.75 + 2.75 TeV	2950	7.1 fm	80 GeV	160 GeV	15 pb	0.15
Xe-Xe	5.86 TeV	30 nb $^{-1}$	2.93 + 2.93 TeV	3150	6.1 fm	100 GeV	200 GeV	7 pb	0.21
Kr-Kr	6.46 TeV	120 nb $^{-1}$	3.23 + 3.23 TeV	3470	5.1 fm	136 GeV	272 GeV	3 pb	0.36
Ar-Ar	6.3 TeV	1.1 pb $^{-1}$	3.15 + 3.15 TeV	3400	4.1 fm	165 GeV	330 GeV	0.36 pb	0.40
O-O	7.0 TeV	3.0 pb $^{-1}$	3.5 + 3.5 TeV	3750	3.1 fm	240 GeV	490 GeV	35 fb	0.11
p-Pb	8.8 TeV	1 pb $^{-1}$	7.0 + 2.75 TeV	7450, 2950	0.7, 7.1 fm	2.45 TeV, 130 GeV	2.6 TeV	0.17 pb	0.17
p-p	14 TeV	1 fb $^{-1}$	7.0 + 7.0 TeV	7450	0.7 fm	2.45 TeV	4.5 TeV	0.18 fb	0.18
Pb-Pb	10.6 TeV	10 nb $^{-1}$	5.3 + 5.3 TeV	5700	7.1 fm	160 GeV	320 GeV	150 pb	1.5
Xe-Xe	11.5 TeV	30 nb $^{-1}$	5.75 + 5.75 TeV	6200	6.1 fm	200 GeV	400 GeV	60 pb	1.8
Kr-Kr	12.5 TeV	120 nb $^{-1}$	6.25 + 6.25 TeV	6700	5.1 fm	260 GeV	530 GeV	20 pb	2.4
Ar-Ar	12.1 TeV	1.1 pb $^{-1}$	6.05 + 6.05 TeV	6500	4.1 fm	320 GeV	640 GeV	1.7 pb	1.9
O-O	13.5 TeV	3.0 pb $^{-1}$	6.75 + 6.75 TeV	7300	3.1 fm	470 GeV	940 GeV	0.11 pb	0.33
p-Pb	18.8 TeV	1 pb $^{-1}$	13.5 + 5.3 TeV	14 400, 5700	0.7, 7.1 fm	4.1 TeV, 160 GeV	4.2 TeV	0.45 pb	0.45
p-p	27 TeV	1 fb $^{-1}$	13.5 + 13.5 TeV	14 400	0.7 fm	4.1 TeV	8.2 TeV	0.30 fb	0.30
Pb-Pb	39 TeV	110 nb $^{-1}$	19.5 + 19.5 TeV	21 000	7.1 fm	600 GeV	1.2 TeV	1.8 nb	200
p-Pb	63 TeV	29 pb $^{-1}$	50. + 19.5 TeV	53 300, 21 000	0.7, 7.1 fm	15.2 TeV, 600 GeV	15.8 TeV	1.5 pb	45
p-p	100 TeV	1 fb $^{-1}$	50. + 50. TeV	53 300	0.7 fm	15.2 TeV	30.5 TeV	0.70 fb	0.70

The possibility to produce the Higgs boson by exploiting the huge photon fields in UPCs of ions,  $AA \xrightarrow{\gamma\gamma} (A)H(A)$ , where the scalar boson is produced at midrapidity and the colliding ions ( $A$ ) survive their electromagnetic interaction (Fig. 1 left), was first considered 30 years ago in several works [9]. Detailed studies of the actual measurement of UPC-production of the Higgs boson in its dominant  $b\bar{b}$  decay mode, including realistic experimental acceptance and efficiencies for the signal and the  $\gamma\gamma \rightarrow b\bar{b}, c\bar{c}, q\bar{q}$  continuum backgrounds (Fig. 1 right), were first presented in Ref. [10] for ultraperipheral proton-nucleus (p-A) and nucleus-nucleus (A-A) collisions at LHC energies. This work showed that, for the nominal integrated luminosities, the scalar boson was unobservable in UPCs at the LHC unless one integrated at least 300 times more luminosity than that expected for the standard 1-month heavy-ion operation. On the other hand, similar studies [11] carried out within the FCC project, have indicated that the observation of Higgs production in UPCs was clearly possible in just the first nominal run of Pb-Pb and p-Pb collisions at  $\sqrt{s_{\text{NN}}} = 39$  and 63 TeV respectively. In this work here, we summarize these previous FCC studies and discuss for the first time the conditions needed for an UPC Higgs boson measurement in the upcoming HL-LHC phase, as well as at the proposed HE-LHC with twice larger c.m. energies, including not only higher luminosities than originally planned for the LHC but also collisions of lighter ions (Xe-Xe, Kr-Kr, Ar-Ar, O-O).

## II. THEORETICAL SETUP

The MADGRAPH 5 (v.2.6.5) Monte Carlo (MC) event generator [12] is employed to compute the UPC Higgs boson and diquark continuum cross sections, following the implementation discussed in detail in [10], as well as to generate the corresponding events for subsequent analysis. The Higgs cross section is obtained from the convolution of the Weizsäcker-Williams EPA photon fluxes for the proton and/or ions, and the elementary  $\gamma\gamma \rightarrow H$  cross section (with H- $\gamma$  coupling parametrized in the Higgs effective field theory [13]), via

$$\sigma_{A_1 A_2 \rightarrow H} = \int dx_1 dx_2 f_{\gamma/A_1}(x_1) f_{\gamma/A_2}(x_2) \hat{\sigma}_{\gamma\gamma \rightarrow H}, \quad (1)$$

where  $x = \omega/E$  is the fraction of the energy of the incoming ion carried by each photon. The same expression is used for the  $b\bar{b}$ ,  $c\bar{c}$ ,  $q\bar{q}$  continuums, where now the elementary  $\hat{\sigma}_{\gamma\gamma \rightarrow b\bar{b}, c\bar{c}, q\bar{q}}$  cross sections at diquark invariant masses around the Higgs mass are directly calculated by MADGRAPH. For protons, the MADGRAPH default  $\gamma$  flux is used, given by the energy spectrum of Ref. [14]:

$$f_{\gamma/p}(x) = \frac{\alpha}{\pi} \frac{1-x+1/2x^2}{x} \int_{Q_{\min}^2}^{\infty} \frac{Q^2 - Q_{\min}^2}{Q^4} |F(Q^2)|^2 dQ^2, \quad (2)$$

where  $\alpha = 1/137$ ,  $F(Q^2)$  is the proton e.m. form factor, and the minimum momentum transfer  $Q_{\min}$  is a function of  $x$  and the proton mass  $m_p$ ,  $Q_{\min}^2 \approx (x m_p)^2/(1-x)$ . For ions of charge  $Z$ , the photon energy spectrum, integrated over impact parameter  $b$  from  $b_{\min} = R_A$  to infinity, is [15]:

$$f_{\gamma/A}(x) = \frac{\alpha Z^2}{\pi} \frac{1}{x} \left[ 2x_i K_0(x_i) K_1(x_i) - x_i^2 (K_1^2(x_i) - K_0^2(x_i)) \right], \quad (3)$$

where  $x_i = x m_N b_{\min}$ ,  $K_0$ ,  $K_1$  are the zero- and first-order modified Bessel functions of the second kind, and for the different nuclear radii  $R_A$ , we use the data from elastic lepton-nucleus collisions [16]. We exclude nuclear overlap by imposing  $b_1 > R_{A_1}$  and  $b_2 > R_{A_2}$  for each photon flux, and applying a correcting factor on the final cross section that depends on the ratio of Higgs mass over  $\sqrt{s_{NN}}$  [17].

After cross section determination, the event generation is carried out for the dominant Higgs decay mode,  $H \rightarrow b\bar{b}$  with 56% branching fraction [18], as it is the final state that provides the largest number of signal events. The same setup is used to generate the exclusive two-photon production of  $b\bar{b}$  and (misidentified)  $c\bar{c}$  and light-quark ( $q\bar{q}$ ) jet pairs, which constitute the most important physical background for the  $H \rightarrow b\bar{b}$  measurement. For the HL-LHC and HE-LHC systems, the analysis is carried out at the parton level only, whereas for FCC energies, we have further used PYTHIA 8.2 [19] to shower and hadronize the two final-state b-jets generated, which are then reconstructed with the Durham  $k_t$  algorithm [20] (exclusive 2-jets final-state) using FASTJET 3.0 [21]. In any case, given that the final state consists just of two quarks (jets) exclusively produced, there are no significant differences between parton- and hadron-level results.

## III. TOTAL HIGGS CROSS SECTIONS

The computed ultraperipheral Higgs boson cross sections as a function of  $\sqrt{s_{NN}}$  are shown in Fig. 2 (left) and listed in the before-last column of Table I for all p-p, p-A, and A-A systems considered. All theoretical cross sections have a conservative 20% uncertainty (not quoted) to cover different charge form factors and nuclear overlap conditions [22, 23]. We note that the quoted cross sections are purely “elastic”, i.e. both incoming ions survive the e.m. interaction. As discussed in [10],  $\gamma\gamma$  interactions can also be “semielastic”, with one (or both) quasireal photons being radiated from individual proton(s), and/or from individual quarks, inside the colliding ions. In this latter case, one (or both) ions breakup at very forward rapidities after photon emission,  $AA \xrightarrow{\gamma\gamma} A H X$ , and the Higgs boson cross sections can be enhanced by about a factor of two compared to the pure elastic results. We do not consider these cases here, and focus on the elastic processes alone. Figure 2 (left) indicates that, as expected, the bigger the charge of the colliding ions the larger the UPC Higgs cross sections, but such an advantage is mitigated in terms of final yields by the correspondingly reduced beam luminosities for heavier ions. Figure 2 (right) shows the product of UPC Higgs cross section times the integrated luminosities for each colliding system in the HL-LHC and HE-LHC energy range. At the LHC, we see that despite the fact that Pb-Pb features the largest Higgs cross section,  $\sigma(\gamma\gamma \rightarrow H) = 15$  pb, there are about 2–3 times more scalar bosons produced per month in Ar-Ar and Kr-Kr

collisions (0.40 versus 0.15, last column of Table I) thanks to the comparatively larger luminosities and c.m. energies of the latter compared to lead beams. At the HE-LHC, the Higgs cross sections are about a factor of 10 larger than at the LHC, and most colliding systems feature 1.5–2.5 Higgs bosons produced per month. The most competitive systems to try a measurement of UPC Higgs production are Ar-Ar at HL-LHC and Kr-Kr at HE-LHC respectively. At the FCC, the cross sections are two orders of magnitude larger than at the LHC, reaching  $\sigma(\gamma\gamma \rightarrow H) = 1.75$  nb and 1.5 pb in Pb-Pb and p-Pb collisions at  $\sqrt{s_{NN}} = 39$  and 63 TeV which, for the nominal  $\mathcal{L}_{int} = 110$  nb $^{-1}$  and 29 pb $^{-1}$  per-month integrated luminosities, yield  $\sim 200$  and 45 Higgs bosons (corresponding to 110 and 25 bosons in the  $b\bar{b}$  decay mode, respectively).

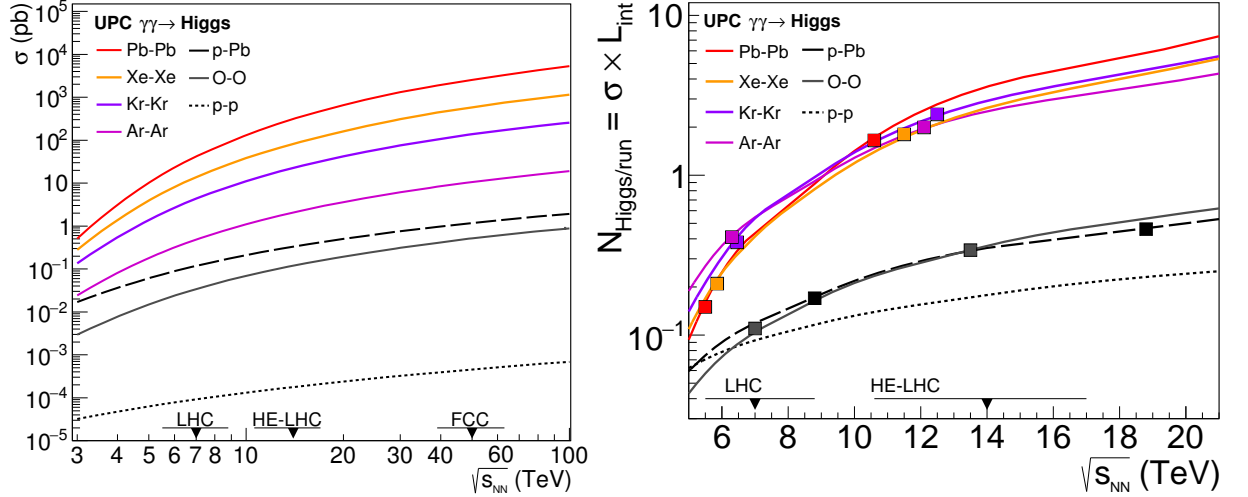


FIG. 2. Left: Two-photon fusion Higgs boson cross section versus nucleon-nucleon c.m. energy in nuclear and proton collisions over  $\sqrt{s_{NN}} = 3$ –100 TeV. Right: Number of Higgs bosons produced per run (according to the integrated luminosities  $\mathcal{L}_{int}$  listed in Table I) in UPCs of various colliding systems in the HL-LHC and HE-LHC energy range. The square symbols indicate the nominal  $\sqrt{s_{NN}}$  for each colliding system.

#### IV. DATA ANALYSIS AND HIGGS BOSON SIGNIFICANCES

The observation of the Higgs boson in UPCs relies on the measurement of two exclusive b-jets with invariant masses peaked at  $m_H$ , on top of a background of exclusive  $\gamma\gamma \rightarrow b\bar{b}, c\bar{c}, q\bar{q}$  continuum pairs, where charm and light ( $q = u, d, s$ ) quarks are misidentified as b-quarks. For all colliding systems, the pure MC-level background continuum cross sections over  $m_H \approx 100$ –150 GeV, computed with the same MADGRAPH 5 setup described above, are about 25, 200, and 500 times larger respectively than the Higgs signal. Experimentally, triggering the online selection of such type of events is straightforward given their unique signature characterized by two back-to-back high transverse momentum ( $p_T$ ) jets in an otherwise empty detector. The data analysis follows closely the study of Ref. [10], to which we refer the interested reader for all details. The following acceptance and reconstruction performances have been assumed: jet reconstruction over  $|\eta| < 2$  ( $< 5$  for FCC), 7% b-jet energy resolution (resulting in a dijet mass resolution of  $\sigma_{jj} \approx 6$  GeV at the Higgs peak), 70% b-jet tagging efficiency, and 5% (1.5%) b-jet mistagging probability for a c (light-flavour q) quark. We note that the b-jet reconstruction and identification performances are expected to be better in the very “clean” exclusive environment of UPCs than in the current high-pileup p-p collisions at the LHC [24]. The pseudorapidity acceptance cut  $|\eta| < 2$  used for HL-LHC and HE-LHC keeps a large fraction of signal jets (around 80%), while removing 2/3 of the background jets, which are much more forward/backward-peaked. In terms of jet (mis)tagging efficiencies, for the double b-jet final-state of interest, these lead to a  $\sim 50\%$  efficiency for the MC-generated signal ( $\mathcal{S}$ ), and a total reduction of the misidentified  $c\bar{c}$  and  $q\bar{q}$  continuum backgrounds ( $\mathcal{B}$ ) by factors of  $\sim 400$  and  $\sim 4500$  respectively. The sum of remaining continuum backgrounds can be further reduced through proper kinematical cuts by requiring [10]: (i) both jets to have transverse momenta around half the Higgs mass,  $p_T \approx m_H/2 \approx 55$ –67 GeV, as expected for jets from the decay of an UPC Higgs produced almost at rest, thereby suppressing more than 95% of the continuum, while removing about half of the signal; (ii) the angle of the jets to be within  $|\cos \theta_{j_1 j_2}| < 0.5$  — to exploit the fact that the angular distribution in the helicity frame of the Higgs decay b-jets is isotropic while the continuum (with quarks propagating in the  $t$ - or  $u$ - channels) is peaked in the

forward-backward directions — further suppressing the backgrounds while leaving almost untouched the number of signal events; and (iii) the pair jet mass to be within  $\pm 1.4\sigma_{jj}$  around the Higgs mass (i.e.  $116 \lesssim m_{b\bar{b}} \lesssim 134$  GeV). For all systems, the overall loss of Higgs signal events due to the acceptance and kinematical cuts (i.e. without accounting for (mis)identification efficiencies) is around a factor of two, whereas the backgrounds are reduced by factors of 30 to 100, resulting in a final  $\mathcal{S}/\mathcal{B} \approx 1$  for all colliding species. We note that any theoretical uncertainty impacts in a similar way the expected yields for signal and background, and thereby leaves the  $\mathcal{S}/\mathcal{B}$  ratio basically unaffected. More advanced multivariate studies could be contemplated, rather than the simpler “cut-based” criteria applied here, that could further improve the separation of signal over background.

Table II lists the cross sections after each event selection step, as well as the final number of events expected (for the nominal integrated luminosities per run) for signal and backgrounds in the systems with larger signal strength at each collider (Fig. 2, right): Ar-Ar at  $\sqrt{s_{\text{NN}}} = 6.3$  TeV, Kr-Kr at  $\sqrt{s_{\text{NN}}} = 12.5$  TeV, and Pb-Pb at  $\sqrt{s_{\text{NN}}} = 39$  TeV. Since the FCC case has been studied in detail in [11], we include also for completeness in the bottom of the table the results obtained for p-Pb at  $\sqrt{s_{\text{NN}}} = 63$  TeV. The listed Pb-Pb and p-Pb results at FCC are those obtained in the full MC analysis described in Ref. [11]. The last column of Table II lists the final number of signal and background events expected after all selection criteria for the nominal 1-month ( $10^6$  s) run operation. The expected number of Higgs per month, after cuts, at the HL-LHC and HE-LHC are below unity, whereas one expects 5 to 20 reconstructed  $H(b\bar{b})$  events at the FCC.

TABLE II. Summary of the cross sections after each event selection step (see text for details), and final number of events expected (for the nominal integrated luminosities quoted) for signal and backgrounds in the  $\gamma\gamma \rightarrow H(b\bar{b})$  measurements in Ar-Ar at HL-LHC, Kr-Kr at HE-LHC, and Pb-Pb and p-Pb at FCC.

Ar-Ar at $\sqrt{s_{\text{NN}}} = 6.3$ TeV	cross section	visible cross section	$N_{\text{evts}}$
	(b-jet (mis)tag effic.)	after $\eta^j, p_T^j,  \cos \theta_{jj} , m_{jj}$ cuts	( $\mathcal{L}_{\text{int}} = 1.1 \text{ pb}^{-1}$ )
$\gamma\gamma \rightarrow H \rightarrow b\bar{b}$	0.20 pb (0.10 pb)	0.045 pb	0.05
$\gamma\gamma \rightarrow b\bar{b}$ [ $m_{b\bar{b}}=100\text{--}150$ GeV]	8.2 pb (4.0 pb)	0.06 pb	0.06
$\gamma\gamma \rightarrow c\bar{c}$ [ $m_{c\bar{c}}=100\text{--}150$ GeV]	61 pb (0.15 pb)	0.005 pb	0.006
$\gamma\gamma \rightarrow q\bar{q}$ [ $m_{q\bar{q}}=100\text{--}150$ GeV]	70 pb (0.016 pb)	$< 10^{-3}$	$< 10^{-3}$
Kr-Kr at $\sqrt{s_{\text{NN}}} = 12.5$ TeV			$N_{\text{evts}}$
			( $\mathcal{L}_{\text{int}} = 0.12 \text{ pb}^{-1}$ )
$\gamma\gamma \rightarrow H \rightarrow b\bar{b}$	11 pb (5.5 pb)	2.5 pb	0.30
$\gamma\gamma \rightarrow b\bar{b}$ [ $m_{b\bar{b}}=100\text{--}150$ GeV]	364 pb (178 pb)	2.8 pb	0.34
$\gamma\gamma \rightarrow c\bar{c}$ [ $m_{c\bar{c}}=100\text{--}150$ GeV]	2.7 nb (6.7 pb)	0.24 pb	0.03
$\gamma\gamma \rightarrow q\bar{q}$ [ $m_{q\bar{q}}=100\text{--}150$ GeV]	3.1 nb (0.70 pb)	$< 10^{-3}$	$< 10^{-4}$
Pb-Pb at $\sqrt{s_{\text{NN}}} = 39$ TeV			$N_{\text{evts}}$
			( $\mathcal{L}_{\text{int}} = 110 \text{ nb}^{-1}$ )
$\gamma\gamma \rightarrow H \rightarrow b\bar{b}$	1.0 nb (0.50 nb)	0.19 nb	21.1
$\gamma\gamma \rightarrow b\bar{b}$ [ $m_{b\bar{b}}=100\text{--}150$ GeV]	24.3 nb (11.9 nb)	0.23 nb	25.7
$\gamma\gamma \rightarrow c\bar{c}$ [ $m_{c\bar{c}}=100\text{--}150$ GeV]	525 nb (1.31 nb)	0.02 nb	2.3
$\gamma\gamma \rightarrow q\bar{q}$ [ $m_{q\bar{q}}=100\text{--}150$ GeV]	590 nb (0.13 nb)	0.002 nb	0.25
p-Pb at $\sqrt{s_{\text{NN}}} = 63$ TeV			$N_{\text{evts}}$
			( $\mathcal{L}_{\text{int}} = 29 \text{ pb}^{-1}$ )
$\gamma\gamma \rightarrow H \rightarrow b\bar{b}$	0.87 pb (0.42 pb)	0.16 pb	4.8
$\gamma\gamma \rightarrow b\bar{b}$ [ $m_{b\bar{b}}=100\text{--}150$ GeV]	21.8 pb (10.7 pb)	0.22 pb	6.3
$\gamma\gamma \rightarrow c\bar{c}$ [ $m_{c\bar{c}}=100\text{--}150$ GeV]	410 pb (1.03 pb)	0.011 pb	0.3
$\gamma\gamma \rightarrow q\bar{q}$ [ $m_{q\bar{q}}=100\text{--}150$ GeV]	510 pb (0.114 pb)	0.001 pb	0.04

The final significance of the signal can be derived from the number of counts within  $\pm 1.4\sigma_{jj}$  around the Gaussian Higgs peak (i.e.  $116 \lesssim m_{b\bar{b}} \lesssim 134$  GeV) over the dijet continuum remaining after cuts. In a simplified cut-and-count approach, one can estimate the statistical sample increase needed for a  $3\sigma$  evidence from the  $N_{\text{evts}}$  values listed in the last column of Table II. For an integrated luminosity two-hundred times larger than the nominal for Ar-Ar(6.3 TeV), one has  $\mathcal{S}/\sqrt{\mathcal{B}} \approx 10/\sqrt{12} \approx 3$ . The same numbers at the HE-LHC, for thirty times more luminosity integrated in Kr-Kr(12.5 TeV), yield  $\mathcal{S}/\sqrt{\mathcal{B}} \approx 9/\sqrt{10} \approx 3$ . Thus, reaching  $3\sigma$  evidence of UPC Higgs-production at HL-LHC and at HE-LHC, requires at least factors of  $\times 200$  and  $\times 30$  more integrated luminosities in Ar-Ar and Kr-Kr collisions, respectively, than currently designed. Figure 3 shows the expected invariant dijet mass distributions after selection criteria for signal and backgrounds at the HL-LHC (Ar-Ar, left) and HE-LHC (Kr-Kr, right) for such increased integrated luminosities. A factor of ten increase in  $\mathcal{L}_{\text{int}}$  could be gained at both colliders simply by running during

the time ( $10^7$  s) typical of a proton-proton run, instead of the nominal 1-month ( $10^6$  s) heavy-ion run operation. Such a longer run, motivated by Higgs- rather than heavy-ion physics, would allow for an evidence of the process at HE-LHC, by combining three experiments (or over three runs in a single one). Achieving the same significance at the HL-LHC seems out of reach, unless an extra factor of twenty in the instantaneous Ar-Ar luminosity is accomplished by some currently unidentified means. In any case, going from the simple evidence to a  $5\sigma$  observation would require yet another extra  $(5/3)^2 \approx 2.8$  increase in the collected data. These estimates indicate that the UPC Higgs observation will very likely remain elusive at the HL-LHC and HE-LHC.

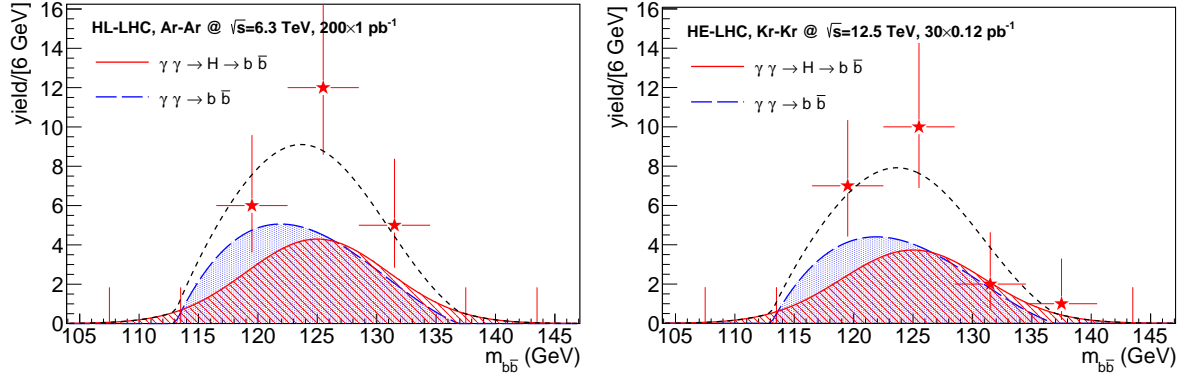


FIG. 3. Expected invariant mass distributions for b-jet pairs from photon-fusion Higgs signal (hatched red Gaussian) and  $b\bar{b} + c\bar{c} + q\bar{q}$  continuum (hatched blue area) in ultraperipheral Ar-Ar ( $\sqrt{s_{NN}} = 6.3$  TeV, left) and Kr-Kr ( $\sqrt{s_{NN}} = 12.5$  TeV, right) collisions, after event selection criteria and with the quoted integrated luminosities (see text). The dashed black curve corresponds to the sum of theoretical signal and background yields.

The situation appears much more favorable at the FCC thanks to the factors ten and one-hundred larger Higgs cross sections, and factors ten increased instantaneous luminosities, compared to the HE-LHC and HL-LHC. Figure 4 presents the expected double b-jet invariant mass distributions in p-Pb (left) and Pb-Pb (right) at the FCC derived in [11]. Lead-lead collisions at  $\sqrt{s} = 39$  GeV with the nominal integrated luminosity of  $\mathcal{L}_{\text{int}} = 110 \text{ nb}^{-1}$  per month, yield  $\sim 20$  signal counts over about the same number for the sum of backgrounds in a  $m_{b\bar{b}} \approx 116\text{--}134$  GeV window. Reaching a  $5\sigma$  statistical significance would just require to combine the measurements of the first run from two different experiments or accumulating two 1-month runs in a single one (Fig. 4, right). Similar estimates for p-Pb at 63 TeV yield about 5 signal events after cuts over a background of 7 continuum events for the design  $\mathcal{L}_{\text{int}} = 29 \text{ pb}^{-1}$ . Reaching a  $5\sigma$  observation of  $\gamma\gamma \rightarrow H$  production requires in this case to run for  $\sim 8$  months ( $10^7$  s), instead of the nominal 1-month, or running 4 months and combining two experiments (Fig. 4, left).

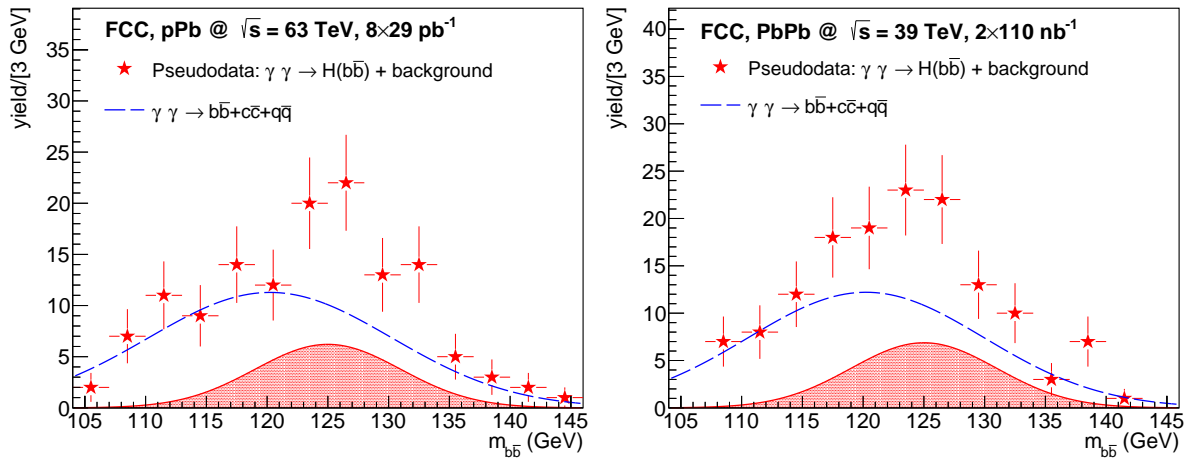


FIG. 4. Expected invariant mass distributions for b-jet pairs from photon-fusion Higgs signal (hatched red Gaussian) and  $b\bar{b} + c\bar{c} + q\bar{q}$  continuum (blue curve) in ultraperipheral p-Pb ( $\sqrt{s_{NN}} = 63$  TeV, left) and Pb-Pb ( $\sqrt{s_{NN}} = 39$  TeV, right) collisions, after event selection criteria and with the quoted integrated luminosities (see text) [11].



All the derived number of events and significances are based on the aforementioned simple set of kinematical cuts and signal-over-background estimates, and can be likely further improved by using more advanced multivariate studies and a full parametric shape analysis for the significance calculation. Notwithstanding such potential improvements, the numbers presented here provide realistic estimates of the feasibility of the UPC Higgs boson measurements at the three future hadron colliders.

## V. SUMMARY

We have presented prospect studies for the measurement of the two-photon production of the Higgs boson in ultraperipheral Pb-Pb, Xe-Xe, Kr-Kr, Ar-Ar, O-O, p-Pb, and p-p collisions at three planned CERN future hadron colliders: HL-LHC, HE-LHC, and FCC. Cross sections have been obtained with MADGRAPH 5, modified to include the corresponding nuclear equivalent photon fluxes with no hadronic overlap of the colliding beams, for nucleon-nucleon c.m. energies over  $\sqrt{s_{NN}} = 3\text{--}100$  TeV. The Higgs cross sections roughly rise by a factor of ten (one hundred) when increasing the c.m. energy from the HL-LHC to the HE-LHC (FCC). At the HL-LHC and HE-LHC, although Pb-Pb features the largest Higgs cross section,  $\sigma(\gamma\gamma \rightarrow H) = 15$ , and 150 pb thanks to its  $Z^4$ -amplified photon fluxes, the most competitive systems to try a measurement of UPC Higgs production are Ar-Ar and Kr-Kr respectively, thanks to the larger available beam luminosities for such lighter species.

The observation of the Higgs boson in UPCs, via its dominant  $b\bar{b}$  decay channel, relies on the measurement of two exclusive b-jets with invariant masses peaked at  $m_H$ , on top of a background of  $\gamma\gamma \rightarrow b\bar{b}, c\bar{c}, q\bar{q}$  continuum pairs, where charm and light ( $q = u, d, s$ ) quarks are misidentified as b-quarks. The same MADGRAPH 5 setup used to compute Higgs cross sections and generate the corresponding events has been employed for the exclusive two-photon production of  $b\bar{b}$ ,  $c\bar{c}$ , and  $q\bar{q}$  dijets. The HL-LHC and HE-LHC analyses have been carried out at the parton level, whereas for FCC energies the b-quarks have been showered and hadronized with PYTHIA 8, and reconstructed in a exclusive two-jet final-state with the  $k_T$  algorithm. By assuming realistic jet acceptance, reconstruction performances, and (mis)tagging efficiencies, and applying appropriate kinematical cuts on the jet  $p_T$  and angles, it has been shown that the  $H(b\bar{b})$  signal can be reconstructed on top of the  $\gamma\gamma \rightarrow b\bar{b}, c\bar{c}, q\bar{q}$  continuum backgrounds. On the one hand, reaching  $3\sigma$  evidence of UPC Higgs-production at HL-LHC and at HE-LHC, requires factors of about  $\times 200$  and  $\times 30$  more integrated luminosities in Ar-Ar and Kr-Kr collisions, respectively, than currently planned for both machines. Factors of ten in integrated luminosity can be gained running for the duration ( $10^7$  s) typical of a proton-proton run, rather than the nominal 1-month heavy-ion operation. This would open up the possibility of a  $3\sigma$  evidence at the HE-LHC, but would still fall too short for any feasible measurement at the HL-LHC. On the other hand, the measurement of  $\gamma\gamma \rightarrow H \rightarrow b\bar{b}$  would yield about 20 (5) signal counts after cuts in Pb-Pb (p-Pb) collisions for their nominal integrated luminosities per run. Observation of the photon-fusion Higgs production at the  $5\sigma$ -level is achievable in the first FCC run by combining the measurements of two experiments (or doubling the luminosity in a single one) in Pb-Pb, and by running for about 8 months (or 4 months and combining two experiments) in the p-Pb case. The feasibility studies presented here indicate the Higgs physics potential open to study in  $\gamma\gamma$  ultraperipheral ion collisions at current and future CERN hadron colliders, eventually providing an independent measurement of the H- $\gamma$  coupling not based on Higgs decays but on a s-channel production mode.

**Acknowledgments** – P. R. T. acknowledges financial support from the CERN TH Department and from the FCC project. We thank I. Helenius and L. Harland-Lang for useful discussions on PYTHIA 8 and/or photon-photon collisions, as well as J. Jowett for feedback on running conditions for light-ions at the HL-LHC and HE-LHC, and E. Chapon on statistical methods.

- 
- [1] C. von Weizsäcker, Z. Physik **88** (1934) 612; E. J. Williams, Phys. Rev. **45** (1934) 729; E. Fermi, N. Cimento **2** (1925) 143.
  - [2] C. A. Bertulani and G. Baur, Phys. Rept. **163** (1988) 299.
  - [3] A. J. Baltz *et al.*, Phys. Rept. **458** (2008) 1 [arXiv:0706.3356 [nucl-ex]].
  - [4] Z. Citron *et al.*, arXiv:1812.06772 [hep-ph].
  - [5] A. Abada *et al.* [FCC Collaboration], CERN-ACC-2018-0059.
  - [6] A. Dainese *et al.*, CERN Yellow Report **3** (2017) 635, [arXiv:1605.01389 [hep-ph]]; D. d’Enterria *et al.*, Nucl. Phys. A **967** (2017) 888 [arXiv:1704.05891 [hep-ex]]; and A. Abada *et al.* [FCC Collaboration], CERN-ACC-2018-0058.
  - [7] M. G. Albrow *et al.* [FP420 R&D Collaboration], JINST **4** (2009) T10001 [arXiv:0806.0302 [hep-ex]].

- [8] S. Chatrchyan *et al.* [CMS Collaboration], Phys. Lett. B **716** (2012) 30 [arXiv:1207.7235 [hep-ex]]; G. Aad *et al.* [ATLAS Collaboration], Phys. Lett. B **716** (2012) 1 [arXiv:1207.7214 [hep-ex]].
- [9] M. Grabiak *et al.*, J. Phys. G **15** (1989) L25; E. Papageorgiu, Phys. Rev. D **40** (1989) 92; M. Drees *et al.*, Phys. Lett. B **223** (1989) 454; K. J. Abraham *et al.*, Phys. Lett. B **251** (1990) 186.
- [10] D. d'Enterria and J. P. Lansberg, Phys. Rev. D **81** (2010) 014004 [arXiv:0909.3047 [hep-ph]].
- [11] D. d'Enterria, D. E. Martins and P. Rebello Teles, CERN-Proceedings-2018-001.33 [arXiv:1712.10104 [hep-ph]].
- [12] J. Alwall *et al.*, JHEP **07** (2014) 079 [arXiv:1405.0301 [hep-ph]].
- [13] M. A. Shifman, A. I. Vainshtein, M. B. Voloshin and V. I. Zakharov, Sov. J. Nucl. Phys. **30**, 711 (1979) [Yad. Fiz. **30** (1979) 1368]; B. A. Kniehl and M. Spira, Z. Phys. C **69** (1995) 77; S. Dawson and R. Kauffman, Phys. Rev. D **49** (1994) 2298.
- [14] V. M. Budnev, I. F. Ginzburg, G. V. Meledin, V. G. Serbo, Phys. Rept. **15** (1975) 181.
- [15] J.D. Jackson, *Classical Electrodynamics*, 2nd edition, John Wiley & Sons (1975).
- [16] H. De Vries, C. W. De Jager and C. De Vries, Atom. Data Nucl. Data Tabl. **36** (1987) 495.
- [17] R. N. Cahn and J. D. Jackson, Phys. Rev. D **42** (1990) 3690.
- [18] M. Spira, Nucl. Instrum. Meth. A **389** (1997) 357 [hep-ph/9610350]; A. Djouadi, J. Kalinowski and M. Spira, Comput. Phys. Commun. **108** (1998) 56 [hep-ph/9704448]; A. Djouadi, J. Kalinowski, M. Mühlleitner and M. Spira, arXiv:1003.1643 [hep-ph];
- [19] T. Sjöstrand *et al.*, Comput. Phys. Commun. **191** (2015) 159.
- [20] S. Catani, Y. L. Dokshitzer, M. H. Seymour and B. R. Webber, Nucl. Phys. B **406** (1993) 187.
- [21] M. Cacciari, G. P. Salam and G. Soyez, Eur. Phys. J. C **72** (2012) 1896 [arXiv:1111.6097 [hep-ph]].
- [22] S. R. Klein *et al.*, Comput. Phys. Commun. **212** (2017) 258 [arXiv:1607.03838 [hep-ph]].
- [23] L. A. Harland-Lang, V. A. Khoze and M. G. Ryskin, Eur. Phys. J. C **79** (2019) 39 [arXiv:1810.06567 [hep-ph]].
- [24] A. M. Sirunyan *et al.* [CMS Collaboration], JINST **13** (2018) P05011 [arXiv:1712.07158 [physics.ins-det]].